Kinetic Simulations of Fast Ions in Stellarators

A. Bustos[1,2], F. Castejón[1,2], M. Osakabe[3], L. A. Fernández[2,4], V. Martin-Mayor[2,4]
[1] *National Fusion Laboratory,*
EURATOM-CIEMAT, 28040 Madrid, Spain
[2] *BIFI, Zaragoza, Spain*
[3] *National Institute for Fusion Science,*
322-6 Oroshi-cho, Toki 509-5292, Japan
[4] *Complutense University, Madrid, Spain*

The steady state distribution function of NBI fast ions is calculated numerically for the LHD and TJ-II stellarators using the code ISDEP (Integrator of Stochastic Differential Equations for Plasmas). ISDEP is an orbit code that solves the guiding center motion of fast ions using Cartesian coordinates in position space, allowing arbitrary magnetic configurations and the reentering of particles in the plasma. It takes into account collisions of fast ions with thermal ions and electrons using the Boozer and Kuo-Petravic collision operator. The steady state distribution function is computed with a time integral following Green's function formalism for a time independent source. The rotation profiles of the fast ions are also estimated, thus computing their contribution to the total plasma current. In addition, energy slowing down time and escape distribution are studied in detail for both devices.

I. INTRODUCTION

Neutral Beam Injection (NBI) heating plays a crucial role in the physics of most fusion devices, since it is a valuable method for plasma heating and fueling and could be very useful for driving current and momentum. The heating and the current drive efficiency depend strongly on their transport parameters. In the present work, the NBI fast ion distribution function is calculated numerically for LHD and TJ-II [2] plasmas using the orbit code ISDEP (Integrator of Stochastic Differential Equations for Plasmas) [3]. Using Green's function formalism, the steady state distribution function is calculated.

The fast ion population is considered as a perturbation to a static plasma background and its dynamics given by the guiding center motion and collisions with thermal ions and electrons. Even thought fast ions are in the low collisionality regime, the complexity of the magnetic field in 3D devices implies that a numerical solution of the fast ion transport is mandatory. ISDEP is an orbit Monte Carlo code that solves the Fokker-Planck equation for the test particle population integrating ion guiding center equations of motion in the 5D phase space: (x, y, z, v^2, λ). The Boozer-Kuo Petravic collision operator for ion-ion and ion-electron collisions with the background plasma is implemented in ISDEP. The code avoids approximations on the size of the orbits and on the diffusive nature of transport. ISDEP uses Cartesian coordinates, allowing to include geometries with magnetic islands or ergodic zones as well as the scrape-off-layer volume where the field lines are open. As a consequence, the properties of collisional ion transport in the whole device can be studied as well as the hit points of escaping ions on the vacuum chamber, as was done in Ref. [4] for TJ-II. These collisions with the vacuum vessel are the only test particle losses in this work since reentering particles are taken into account. The equations of motion and details about the code can be found in [3]. On the other hand, ISDEP usually requires more CPU time than magnetic coordinates-based codes since the equations of motion in Cartesian coordinates are much more complicated.

The steady state distribution function is calculated for a stationary source. This is a good approximation for the NBI heating in which the injectors launch an almost constant current of neutrals with constant energy spectrum. In this work two different situations are considered: perpendicular beam injection for LHD and tangential injection for TJ-II. Comparison with experimental data will be done in future works.

The remaining part of this paper is organized as follows: in Section II the LHD and TJ-II plasmas and the NBI initial condition are described. In Section III the steady state distribution function is calculated for the fast ion population in the two devices. Section IV and V are devoted to the study of rotation, slowing down and escape points of the test particles. Finally we present our conclusions in Section VI.

II. PLASMA AND INITIAL CONDITIONS

The plasma background equilibrium in the two stellarators studied is obtained with VMEC [5] considering the typical plasma profiles for this type of discharges. The scrape-off-layer profiles are estimated with an extrapolation of the equilibrium profiles. An exponential decay outside the plasma is assumed for density and temperature profiles, while the electric potential is kept constant.

Although in LHD most of the NBI heating power comes from tangential injection, in this work we simulate fast ions injected perpendicularly by NBI line number 4 (6 MW power). Line 4 is especially valuable for future comparisons with experimental data. The ions are initialized following the distribution function provided by the code HFREYA [6]. HFREYA is a Monte Carlo code that estimates the dynamics of fast neutrals inside the plasma, including propagation, ionisation and charge exchange. The distribution function provided by HFREYA presents three peaks in energy at $\sim$ 36, 18 and 12 keV, as can be seen in Fig. 1. The pitch angle distribution function is roughly Gaussian centered close to 0. HFREYA provides a list of fast ion birth points in phase space ($\sim 10^5$ events). ISDEP chooses randomly the initial condition from that list, which is known as the bootstrap method in Monte Carlo studies.

In the LHD simulations the electric field is neglected since it is too small to have consequences on the orbits of such fast ions. Fig. 1 also shows the plasma equilibrium profiles. The plasma parameters are roughly $T_i = T_e \sim 1 - 2\,\mathrm{keV}$, $n \sim 2 \cdot 10^{19}\,\mathrm{m}^{-3}$ for the standard configuration with magnetic axis $R_0 = 3.60\,\mathrm{m}$

TJ-II is equipped with two tangential injectors that launch neutrals in co and counter directions. We simulate here the neutrals injected tangentially with line number 1 (co-directed to the magnetic field). The birth point locations in phase space are estimated with FAFNER2 [7], which is another Monte Carlo code similar to HFREYA. TJ-II simulations with ISDEP do take into account the electric field because it is not negligible in this case. Fig. 2 shows the plasma background profiles for the simulations as well as the energy and pitch angle distribution of the fast ions created from the fast neutrals. In this case the pitch angle distribution is peaked at $\lambda = 1$, since we are dealing with co and tangential injection. The plasma background corresponds to the standard magnetic configuration and typical ECRH discharge profiles: $T_i \sim 100\,\mathrm{eV}$, $T_e \sim 1\,\mathrm{keV}$, $n \sim 0.6 \cdot 10^{19}\,\mathrm{m}^{-3}$. These conditions are representative of the initial phase of an NBI discharge.

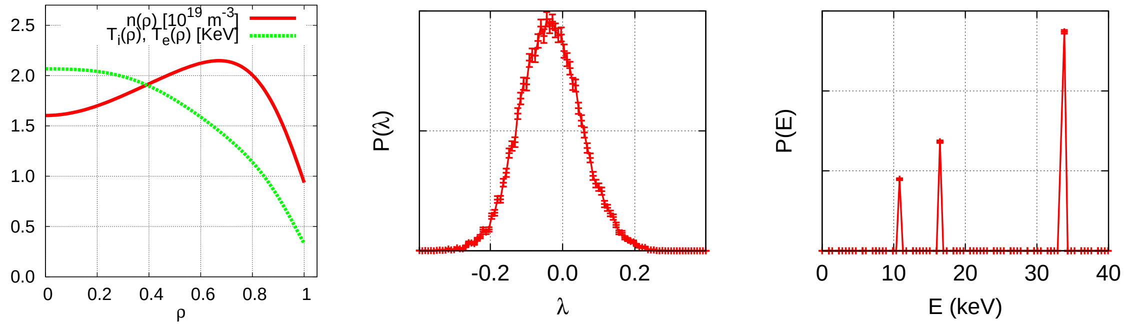

FIG. 1. Density and ion and electron temperature profiles used in the simulations for LHD (left), provided by VMEC. The fast ion initial distribution is given by HFREYA. It is centered in 0 in the pitch (center) and presents three peaks in the energy (right).

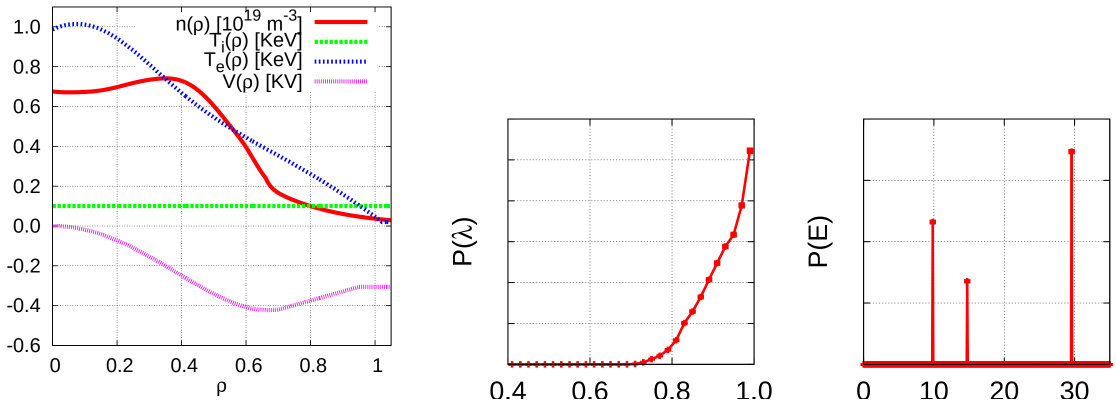

FIG. 2. Same as Fig. 1 for TJ-II.

III. STEADY STATE DISTRIBUTION FUNCTION

Many relevant properties of the fast ion confinement can be obtained taking statistical measurements on the trajectories of the launched particles. In this section we calculate a marginal distribution of the fast ion distribution function $f(t, x, y, z, v^2, \lambda)$. Position space is expressed by means of the effective radius ρ and velocity space in terms of the two components of the velocity $(v_{||}, v_\perp)$. This 4D space is discretized with a 4 dimensional histogram in $(t, \rho, v_{||}, v_\perp)$. Every trajectory contributes to f, increasing the statistics according to the initial state and single particle dynamics. Note that what is obtained with ISDEP is the distribution function multiplied by the jacobian: $f(t, \rho, v_{||}, v_\perp)\cdot J(\rho, v_\perp)$. The steady state of this quantity is calculated with the Green function formalism, following [8]. Let $f(x, t)$ be the distribution function of our system, t the time, x the coordinates in phase space, $\mathcal{L}$ a differential operator over f and $S(x, t)$ the source term. With this notation, the problem is expressed as:

$$\mathcal{L}\left(f(x,t)\right) = S(x,t) \tag{1}$$

In the case of interest $f(x, t)$ is the minority fast ion distribution function, $\mathcal{L}$ is the Fokker Planck operator for the guiding center and Boozer collision operator and the source is the continuous injection of fast ions into the plasma. A Green function $G(x, t; x_0)$ is defined such that

$$\mathcal{L}\left(G(x,t;x_0)\right) = 0, \tag{2}$$

$$\mathcal{L}\left(G(x,0;x_0)\right) = \delta(x - x_0), \tag{3}$$

with x_0 playing the role of initial position. Then:

$$f(x,t) = \int \mathrm{d}t_0\, \mathrm{d}x_0\, G(x, t - t_0; x_0)\, S(x_0, t_0), \tag{4}$$

because

$$\mathcal{L}\left(f(x,t)\right) = \int \mathrm{d}t_0\, \mathrm{d}x_0\, \mathcal{L}\left(G(x, t - t_0; x_0)\right)\, S(x_0, t_0) = S(x,t). \tag{5}$$

Note than the only contribution to this integral comes when $t = t_0$. In the systems studied here the source is assumed to be constant in time. This means that neither the beam line changes with time nor the birth points change because the background plasma is constant. Then $S(x,t) = S(x)$ and Eq. 4 is simplified:

$$f(x,t) = \int \mathrm{d}t_0 d\mathrm{d}x_0\, G(x, t - t_0; x_0)\, S(x_0) \tag{6}$$

$$= \int \mathrm{d}t_0 \int \mathrm{d}x_0\, G(x, t - t_0; x_0)\, S(x_0). \tag{7}$$

Defining

$$H(x,t) = \int \mathrm{d}x_0\, G(x, t; x_0)\, S(x_0), \tag{8}$$

the distribution function is a time integral:

$$f(x,t) = \int \mathrm{d}t_0\, H(x, t - t_0). \tag{9}$$

It is important to remark that this approximation is valid as long as the plasma background is not modified and the number of test particles much smaller than the total number of particles in the plasma. It is correct at the beginning of a discharge, but when the bulk plasma heating and fueling is important it losses its validity.

A. Numerical Scheme

Except for a multiplicative constant, the function $H(x,t)$ is calculated by ISDEP after integrating $\sim 10^5$ test particle trajectories and analyzing the results. The equations of motion and the method used to analyze the set of trajectories can be found in [3]. Around $5 \cdot 10^4$ CPU-hours have been needed, provided by grid and high performance computing. Finally, with a 1D numerical integration, $f(x,t)$ can be easily found. In fact, for sufficiently large times, $f(x,t)$ is expected to be constant in time because of the equilibrium between continuous injection and particle losses, since the persistence of the test particles (defined as the probability of finding a given particle inside the plasma, see Section IV) always goes to zero. The fast ion losses are basic to get the steady state distribution function and in this work an ion is considered to be lost when it hits the vacuum vessel of the device. We take advantage of the capability of ISDEP of following particles in the scrape off layer. In this way the re-entrance of the ions is taken into account in the steady state calculation.
The function $H(x,t)$ does not necessarily have to be a distribution function. It can be any other time dependent quantity of the fast ion population, as the average rotation and radial velocities (Section IV).
Due to its linear nature, ISDEP cannot provide absolute values of f, hence the results are presented normalized so that $\sum_{ijk} J(\rho_i, v_{\perp k}) f(\rho_i, v_{||j}, v_{\perp k}) = 1$ where the indexes i, j, k run over the discretized phase space. Nevertheless, real values can be calculated multiplying f times the incoming flux of particles.

B. Application to LHD and TJ-II

The distribution function of the LHD fast ions calculated following the above shown procedure is plotted in Fig 3 for four radial positions: $\rho = 0.15$, $\rho = 0.45$, $\rho = 0.65$ and $\rho = 0.95$. The error calculation is done using the Jack-Knife technique [9]. This method avoids over estimations of the statistical error of non linear functions of the sample. It is seen that the ions tend to thermalize and spread in velocity space almost symmetrically in $v_{||}$, although some asymmetry is still present. Traces of the continuous injection of high energy ions can be seen at all positions.
In TJ-II the situation is different, as can be seen in Fig. 4. The birth points of test particles are located close to the magnetic axis due to the fact that the background plasma density is too low in the edge. Hence there are not many trajectories of fast ions in the outermost part of the plasma. The injection is tangential to the direction of $\mathbf{B}$, therefore there are not high negative parallel velocities in the distribution and almost all the fast particles appear for positive parallel velocities. A strong dispersion in the pitch angle appears due to the pitch angle scattering. The thermalization of particles is much less effective in TJ-II than in LHD, which makes the distribution function much farther from the Maxwellian than in the case of LHD. It is also necessary to consider the effects of transport: the fast ions that appear at outer positions of TJ-II come from the center of the plasma. Finally, the strong decrease of fast ion density observed at the outermost magnetic surfaces can be understood just considering the direct losses.

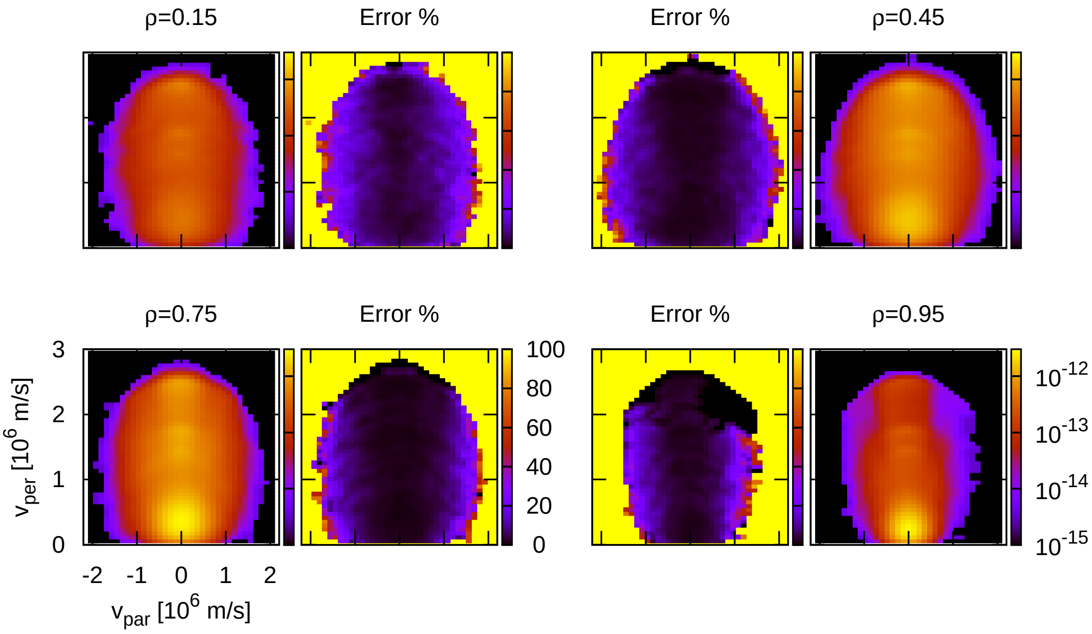

FIG. 3. $J(\rho, v_\perp) \cdot f(\rho, v_{||}, v_\perp)$ and the relative error for four different radial positions in the steady state for LHD.

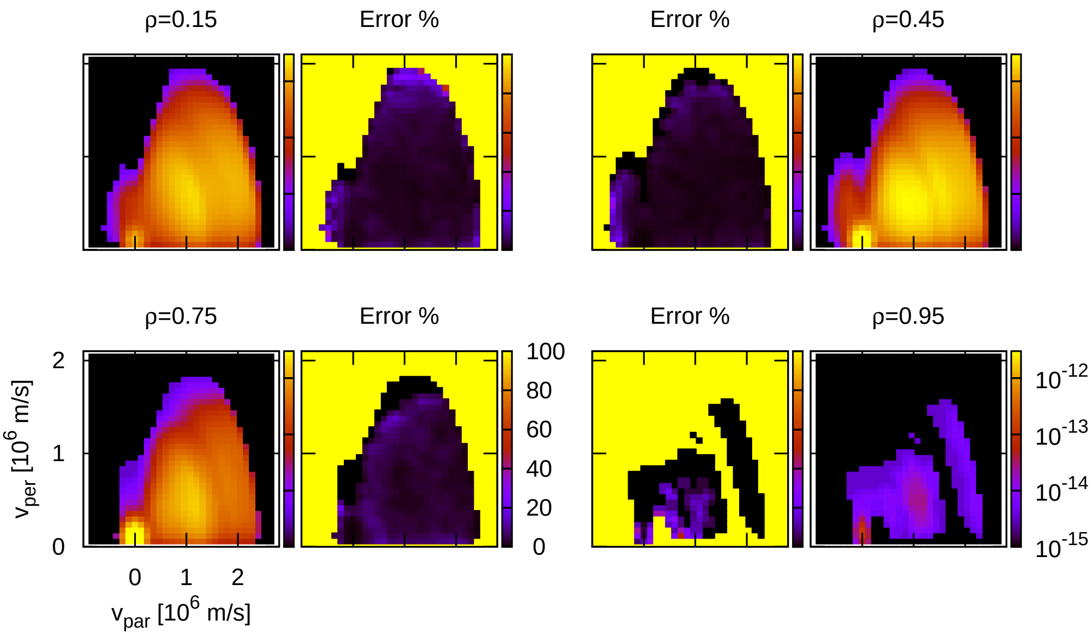

FIG. 4. $J(\rho, v_\perp) \cdot f(\rho, v_{||}, v_\perp)$ for four different radial positions in the steady state for TJ-II.

IV. FAST ION DYNAMICS: ROTATION AND SLOWING DOWN TIME

The study of the toroidal rotation is important because it has strong influence on the confinement, especially in tokamaks where the toroidal rotation can play a crucial role for MHD stabilization (see [10] for a review on toroidal plasma rotation in tokamaks) and where spontaneous rotation, without any input of angular momentum, is observed [11]. It contributes significantly to the total plasma current, modifying then the confining magnetic field. Despite of the fact that the toroidal rotation is especially relevant in tokamaks, it is very useful to perform this study in a

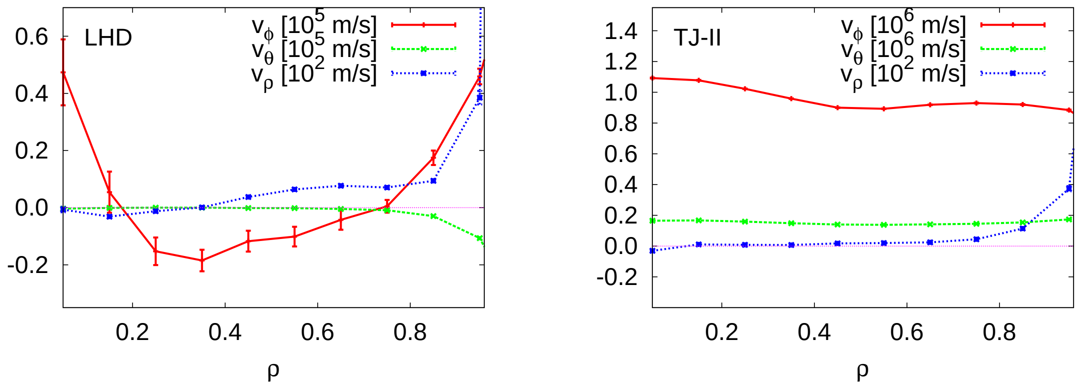

FIG. 5. Toroidal and poloidal rotation and radial velocity profiles for LHD and TJ-II. The two fast ion population rotate in a different way due to the distinct initial conditions.

stellarator where the toroidal rotation is limited and the fast ions are in principle the only momentum source, so it is possible to validate the presented models with experimental data. Moreover, the toroidal rotation in stellarators can also play a relevant role in the plasma stabilization, as has been discussed in Ref. [12], and can also appear spontaneously, without any input of momentum [13]. The poloidal rotation is also relevant for the confinement, since it has been demonstrated that poloidal sheared flows can be beneficial for the confinement, both in tokamaks and stellarators. This mechanism was predicted theoretically in 1990 [14] and was confirmed experimentally in the DIII-D tokamak [15]. The radial transport, and hence the particle confinement, is closely related to the radial velocity. The toroidal, poloidal and radial velocity profiles in the steady state are plotted in Fig. 5 for both LHD and TJ-II.

Despite of the fact that the injection is almost perpendicular for LHD, the toroidal rotation (v_ϕ) is nonzero and presents a strong shear, changing sign twice while moving in the radial direction. The mechanisms that determine this velocity are the initial conditions, the structure of the background magnetic field and the collisionality profiles, in a similar way as the bootstrap current is generated. The poloidal velocity v_θ is almost zero in most of the plasma column and becomes negative for $\rho > 0.8$. The radial velocity v_ρ, proportional to the outward particle fluxes, clearly presents three regions of interest. In the inner region of the plasma is zero or negative, meaning a very good confinement of fast ions. In the region defined by $0.4 < \rho < 0.8$, $v_\rho \sim 1$m/s so the confinement gets worse. Near the border of the plasma where $\rho > 0.8$ the radial transport is higher, showing the effects of ion loses at these positions and a worse confinement of fast ions in the plasma edge.

In the case of TJ-II the results are quite different due to the different characteristics of the device and to the tangential injection. As expected, the average toroidal velocity of the fast ions, v_ϕ, is much higher in TJ-II than in LHD, as can be seen in Fig. 5. In this case the high initial parallel velocity is so large that the influences of the structure of the magnetic field and the collisonality are not enough to reduce it substantially. The poloidal rotation v_θ is almost constant and the relative change of v_ρ along the radius is much smaller that in the LHD case, except in the plasma edge.

The slowing down time of the NBI ions is a very important quantity because it is related to the efficiency of the heating system. The shorter the slowing down time, the more efficient the power absorption by the plasma background and the more reduced the fast ion losses. It is defined as the time that the average energy of the beam takes to reach the background temperature. The energy slowing down time profile is calculated with the data of $f(t, \rho, v_{||}, v_\perp)$ from previous section. An integration gives the energy profile:

$$E(t,\rho) = \int \mathrm{d}v_{||}\,\mathrm{d}v_\perp\, J(\rho, v_\perp) f(t,\rho,v_{||},v_\perp)\frac{m(v_{||}^2+v_\perp^2)}{2}. \tag{10}$$

Assuming that the energy follows an exponential law in time, the slowing down time profile can be found with a fit to:

$$E(t,\rho) = A(\rho) + B(\rho)\mathrm{e}^{-\frac{t}{\tau(\rho)}}. \tag{11}$$

The slowing down time profile is plotted in Fig 6 for the two devices as well as the χ^2 of each fit with Eq. (11). In order to compare our results with the estimations of the neoclassical theory, we follow [16] to calculate the Spitzer

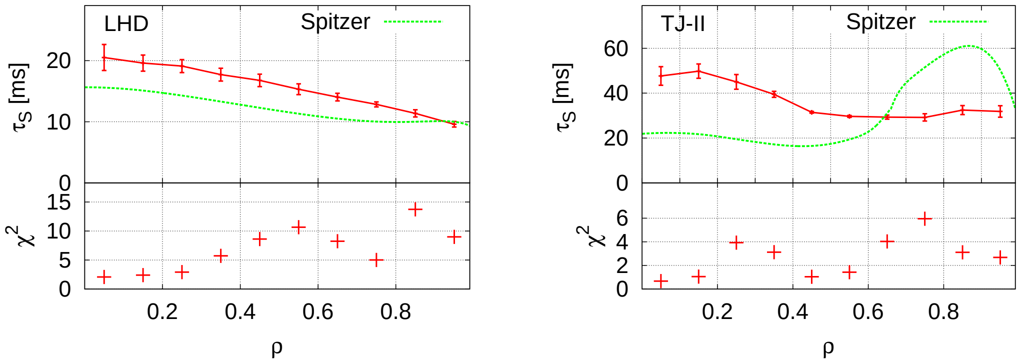

FIG. 6. Slowing down time, calculated with a fit to Eq. 11 and with the Spitzer formula. We plot the χ^2 for each fit. In these fits there are 14 degrees of freedom.

slowing down time:

$$\tau_S = \frac{t_S}{3} \log \left(1 + \left(\frac{W}{W_c} \right)^{3/2} \right), \tag{12}$$

where t_S and W_c are:

$$W_c = 16.0\, T_e, \qquad t_S = 6.27 \cdot 10^2 \frac{T_e^{3/2}}{n_e \log \lambda}. \tag{13}$$

W_c is known as the critical energy, defined as the energy for which the same energy is transferred from the beam to the background ions and electrons. For beam energies above W_c, more power is transferred to the electrons than to the ions. The time t_S is proportional to the inverse of the collision frequency and $\log \lambda$ is the Coulomb logarithm. In LHD the beam energy is close to W_c, but in TJ-II is $\sim 2\, W_c$. In Fig. 6 the slowing down time calculated with ISDEP and Eq. (12) are plotted,

Discrepancies between the two time profiles can be observed in Fig. 6, being stronger for TJ-II than for LHD. These discrepancies can be understood by considering the effect of ion transport in the complex 3D geometry of the devices, especially of TJ-II, which is not taken into account in Spitzer formula. In the ISDEP calculation, the energy slowing down time is estimated including all the fast ion dynamics: transport, particle losses, geometrical features, apart from the collisional processes with thermal particles. It can be seen in Figs. 7,8 (upper left) that the slowing down process occurs in a similar time scale as fast ion confinement time, meaning that the above referred processes are relevant. In TJ-II these discrepancies with the theory are more important because the relation between the typical banana width and the minor radius is much higher than for LHD. Indeed this has consequences on transport and makes fast ions travel along a substantial fraction of the minor radius, making non-local effects relevant [17]. The sudden increase of τ_S calculated with the Spitzer formula near $\rho = 0.6$ is due to the shape of the density and temperature profiles (Fig. 2), which present a strong gradient in that region.

V. ESCAPE DISTRIBUTION AND CONFINEMENT

The main properties of the confinement of fast ions are estimated and shown in this section. The confinement is described by the persistence of the particles, which is a global magnitude, and by the loss cone in velocity space. The persistence of particles is defined as the probability of finding a particle in the plasma after a given time (see [3]), so it provides a measurement of the confinement time of particles. The loss cone is defined as the region of the velocity space where the ions are lost for a given time interval. The reader should notice that the steady state calculations are not needed to obtain these two important characteristics of the confinement of fast ions. The persistence and the loss cones are plotted in Fig. 7 for LHD and in Fig. 8 for TJ-II.

The upper left panel of Fig. 7 shows the time evolution of the persistence of fast ions in LHD. It is clearly seen that the curve cannot be fitted by an exponential, which means that the confinement presents a strong time dependence, showing two different time scales. The big slope in the persistence $P(t)$ at $t \sim 10^{-4}$ s for LHD that is observed in Fig. 7 is caused by prompt losses and corresponds to the first part of ion dynamics. Then a second phase appears,

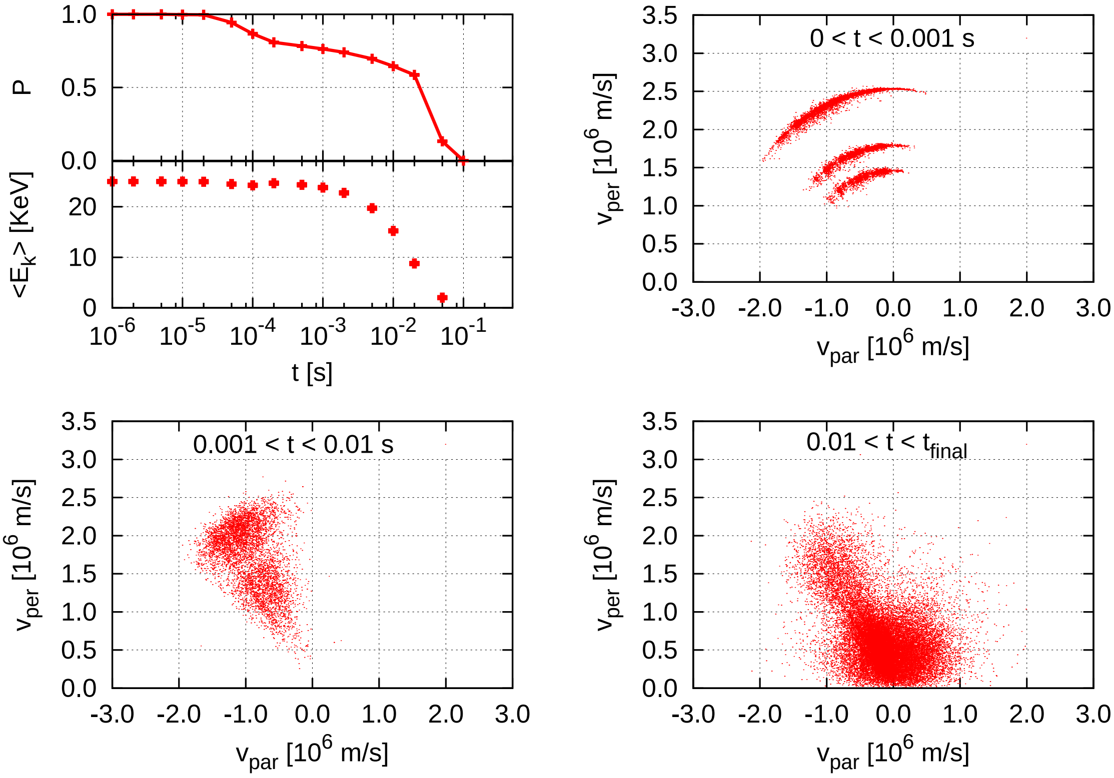

FIG. 7. Particle escape analysis for LHD. In the upper left figure, persistence and average energy for the whole test particles population is plotted as a function of time. In other plots, hit points with the vacuum vessel in velocity space are plotted, showing the spreading of the loss cone with time.

when ions suffer the slowing down process, which increases the bulk of the distribution function (as can be seen in Fig. 3). The average kinetic energy of confined ions is plotted in the same panel, showing that the prompt losses have not a strong effect in this quantity. For times $t > 10^{-2}$ s it is severely degraded when the majority of fast ions suffer the loss of confinement. The loss cones evolves in time and becomes wider as the dispersion of fast ions increases. Despite of the perpendicular injection, the loss cone presents a strong asymmetry at every time scale. This must be attributed to the particular magnetic structure of the device. The asymmetry is, nevertheless, softened by diffusion processes in phase space.

Due to the different initial conditions (remind the tangential injection in TJ-II), prompt losses are much higher in LHD than in TJ-II. In fact, the former ones represent about 20% compared with 5% found in TJ-II. This makes that, differently to what it is found in LHD, the persistence in TJ-II presents roughly a single time scale.

The loss cone in TJ-II shows clearly the different character of the injection. Interestingly, the effect of pitch angle scattering starts being significant for times of the order of $10^{-3} - 10^{-2}s$. For longer times the dispersion caused by pitch-angle scattering is much stronger. It is also shown in Fig. 8 that the loss cone is extended also to the region of negative parallel velocity due to the effects of pitch-angle scattering, showing the appearance of a non negligible amount of ions with negative parallel velocity that finally escape from the plasma.

The energy distribution of losses is plotted in Fig. 9. Two probability densities are calculated for each device: taking into account all escaping particles (with subscript P. L.) and removing the prompt losses (w/o P. L). In agreement with the former results, it is seen that the energy prompt losses are much more important for LHD. Moreover, the average energy of the lost particles is almost three times larger in LHD than in TJ-II.

VI. SUMMARY AND CONCLUSSIONS

The confinement properties of the NBI fast ions are studied for stellarators using the global Monte Carlo guiding center orbit code ISDEP. This code avoids common assumptions on the diffusive nature of transport and on the radial

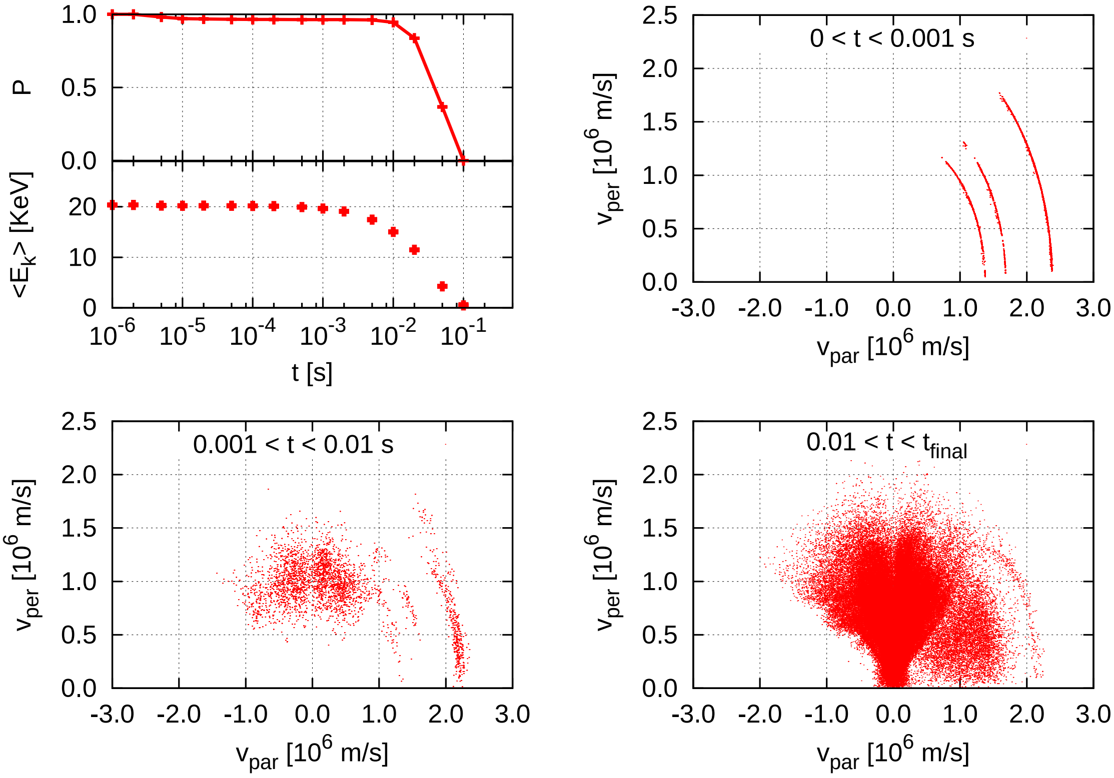

FIG. 8. The same as in Fig. 7 for TJ-II.

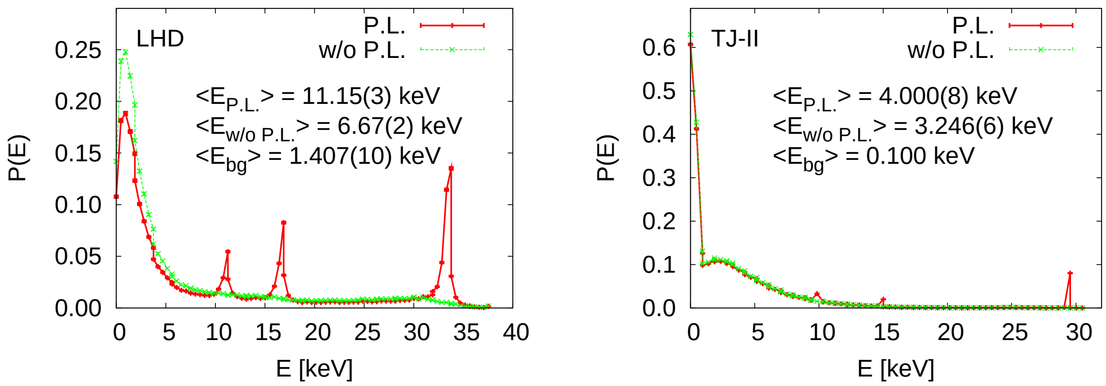

FIG. 9. Energy distribution of losses for LHD and TJ-II. The energy spectra is plotted with and without considering prompt losses of the devices. The three peaks above 10 keV make prompt losses important in LHD. In TJ-II the peak near 30 keV is the only non negligible contribution to this effect.

size of the ion orbits. It also allows to follow particles in the scrape off layer, therefore taking into account phenomena like the re-entrance of ions in the plasma. The steady state is estimated by using Green function techniques.

The main result of this work is the calculation of the fast ion distribution function $f(\rho, v_{||}, v_{\perp})$ for two different NBI lines and plasmas: perpendicular injection for LHD and tangential for TJ-II. All the relevant quantities can be estimated as moments of such a distribution. The steady state profiles of toroidal and poloidal rotation and radial velocity are calculated in this way. The toroidal rotation velocity is the fraction of rotation provided by fast ions, which is important to estimate the NBI capability for rotation driving. The interest of the calculation of poloidal rotation relies particularly on its capability for creating shear flows, which could help to reduce the turbulence and to create transport barriers.

The slowing down time is also computed and compared with Spitzer's formula, showing the effect of the particular

magnetic configuration and injection properties on such a quantity. The loss cones in the two devices are also estimated with ISDEP as functions of time, showing the different time scales of the losing processes. The slowing down time appears to be of the same order of the fast ion confinement time in the two studied cases, which means that the heating efficiency is negatively affected by the lost of ions.
Comparison with experimental data [18, 19] measured with NPA's (Neutral Particle Analyzers) will be done in the near future. From the time evolution of f it is possible to estimate the momentum and energy transfer to the background plasma.

ACKNOWLEDGMENTS

This work has been partially funded by the Spanish Ministerio de Ciencia e Innovacion, Spain, under Projects ENE2008-06082/FTN and FIS2009-12648-C03-0L. The computing resources used in these simulations have been provided by the EULER cluster at CIEMAT and by the Fusion Virtual Organization in the EGEE project.

[1]
[2] C. Alejaldre *et al.*, Fusion Technology **17**, 131 (1990).
[3] F. Castejón *et al.*, Plasma Physics and Controlled Fusion **49**, 753 (2007).
[4] F. Castejón *et al.*, Nuclear Fusion **49**, 085019 (2009).
[5] S. Hirshman and J. Whitson, Physics of Fluids **26**, 3553 (1983).
[6] S. Murakami, N. Nakajima, and M. Okamoto, Fusion Technology **27**, 256 (1995).
[7] J. Teubel, *Monte Carlo simulations of NBI into the TJ-II helical axis stellarator* (Max Planck Institute fur Plasmaphisik, 4/268, Germany, 1994).
[8] S. Murakami *et al.*, Nuclear Fusion **46**, S425 (2006).
[9] D. Amit and V. Martin-Mayor, *Field Theory, the Renormalization Group and Critical Phenomena*, 3rd ed. (World Scientific Publishing, Singapore, 2005).
[10] P. W. Terry, Rev. Mod. Phys. **72**, 109 (2000).
[11] J. Rice *et al.*, Nuclear Fusion **47**, 1618 (2007).
[12] P. Helander and A. N. Simakov, Phys. Rev. Lett. **101**, 145003 (2008).
[13] M. Yoshinuma *et al.*, Nuclear Fusion **49**, 075036 (2009).
[14] H. Biglari, P. H. Diamond, and P. W. Terry, Phys of Fluids B **2**, 1 (1990).
[15] R. J. Groebner, K. H. Burrell, and R. P. Seraydarian, Phys. Rev. Lett. **64**, 3015 (1990).
[16] T. H. Stix, Plasma Physics **14**, 367 (1971).
[17] J. Velasco, F. Castejón, and A. Tarancón, Physics of Plasmas **16**, 052303 (2009).
[18] M. Osakabe *et al.*, Review of Scientific Instruments **79**, 10E519 (2008).
[19] R. Balbin *et al.*, EPS 2005 meeting, Tarragona, Spain, D5.001 (2005).